PET with a Dual-Head Coincidence Camera: Spatial Resolution, Scatter Fraction, and Sensitivity

Wolf-Dietrich Kunze, Manfred Baehre, and Eckhart Richter

Clinic of Radiotherapy and Nuclear Medicine, Medical University of Luebeck, Luebeck, Germany

Scintillation cameras with options for detecting positron annihilation quanta in the coincidence acquisition mode may be the most innovative diagnostic devices introduced in nuclear medicine during the last few years. Besides conventional low-energy imaging in the collimated single-photon mode, these options offer a relatively inexpensive opportunity to perform uncollimated PET by switching into the coincidence acquisition mode. Instead of collimators, scatter frames (with 2 optional configurations: axial or open scatter frame) can be mounted to reduce the amount of quanta reaching the detectors from parts of the patient's body outside the field of view. This study investigates the coincidence imaging properties of the scintillation camera by measuring spatial resolution, scatter fraction, sensitivity, and count-rate response for ^{18}F. **Methods:** A needle in air and a plastic tube in water, each filled with ^{18}F, were oriented axially and transversally to measure the transverse and axial spatial resolutions, respectively. Using either the axial or the open scatter frame, a standard cylinder filled homogeneously with activity was studied over several half-life periods to deduce the respective scatter and random fractions of the system by means of a sinogram technique. The activity of the cylinder was kept low to determine the sensitivity to coincidence events for both scatter frames. **Results:** Depending on the distance between the line source and the axis of rotation and on the choice of the axial acceptance angle used to reconstruct the coincidence events (single-slice rebinning algorithm), the axial resolution was found to be between 6 and 10 mm (full width at half maximum) with the axial scatter frame mounted. The transversal resolution was 6–6.5 mm on the axis of rotation, independent of the scatter frame used. The scatter fraction amounted to roughly 25% for the axial and 38% for the open scatter frames. The sensitivity when measuring true coincidence pairs ran to nearly 650 Hz/kBq/mL, when acquisition was performed with the axial scatter frame using a 30%-wide photopeak energy window. When acquiring with the open scatter frame, the sensitivity increased to nearly 3000 Hz/kBq/mL. Using the axial scatter frame, the homogeneously filled cylinder could be scanned with a maximum true coincidence rate of 2000 Hz for an activity of 55–60 MBq. Although this maximum true coincidence counting rate did not change significantly when the acquisition was performed with the open scatter frame, the respective activity in the standard cylinder was decreased to 10–15 MBq. **Conclusion:** The spatial resolution of the scintillation camera is sufficient for high-resolution coincidence imaging. Compared with a dedicated PET scanner, the scatter fraction is relatively high and should therefore be corrected adequately. The relatively low sensitivity and the rather low maximum true coincidence counting rate are considerably inferior compared with a conventional PET scanner. However, these drawbacks can be partially compensated for, facilitating its clinical use.

Key Words: PET; coincidence scintillation camera; spatial resolution; scatter fraction; sensitivity

J Nucl Med 2000; 41:1067–1074

After the development of the first positron emission tomograph at the Brookhaven nuclear facility (Upton, NY) in 1961, more than 10 y passed before PET was adopted in medical research and diagnosis (*1*). Since that time, the PET camera has undergone a number of improvements. Two of these were single-ring systems for the measurement of individual transversal slices and planar detectors for the simultaneous measurement of several transversal slices (*1*). The most common scintillation crystal was sodium iodide (NaI[Tl]), which was already well known in conventional low-energy nuclear medicine, especially the characteristics of its spatial and energy resolutions. Not long afterward, however, bismuth germanate (BGO) was introduced and found to be more suitable for the efficient detection of coincident 511-keV positron annihilation quanta. In recent years BGO scintillation crystals in block structures were incorporated into full-ring systems, and their use resulted in a marked improvement in spatial resolution and a discernible increase in the sensitivity to annihilation quanta. These detector systems have been optimized exclusively for and are used only with PET.

The objective of the development of PET equipment has always been to optimize the detection of coincident 511-keV quanta with respect to spatial resolution, sensitivity, and contrast. A large number of PET cameras are now available with different geometric arrangements (full rings, partial rings) and several parallel rings oriented in the axial direction, which can be used either individually (2-dimensional PET with extended septa) or in combination (3-dimensional PET with retracted septa) for quanta measurement. In the past few years, cost minimization and extension

Received Jul. 27, 1998; revision accepted May 4, 1999.

For correspondence or reprints, contact: Wolf-Dietrich Kunze, PhD, Clinic of Radiotherapy and Nuclear Medicine, Medical University of Luebeck, Ratzeburger Allee 160, D-23538 Luebeck, Germany.

of the axial fields of view of these cameras have emerged as important criteria for additional PET development. At the same time, several companies have developed relatively inexpensive scintillation cameras that are capable not only of detecting single photons in the low-energy range with collimators but also of detecting coincident 511-keV annihilation quanta.

This article describes a scintillation camera capable of coincidence detection and examines its ability to detect positron annihilation quanta.

MATERIALS AND METHODS

Camera Description

The equipment studied consisted of a dual-head camera (Prism 2000 XP; Picker International, Cleveland, OH) with a coincidence option referred to by the manufacturer as positron coincidence detection. A 0.75-in. (19-mm) NaI(Tl) scintillation crystal was used. The use of NaI(Tl) permited high-resolution imaging with low-energy photons (^{201}Tl, ^{99m}Tc) and collimators, and the doubling of the thickness of the crystal to 0.75-in. (19-mm) increased its efficiency in detecting coincident 511-keV photons. Compared with a 0.375-in. (9.5-mm) crystal, the probability of photoelectric events for single 511-keV quanta was increased from 12% to 26% and that for coincident 511 keV quanta from 1.4% to 6.8% (*2*).

The 2 camera heads each had a field of view of 368 mm in the axial and 508 mm in the transversal direction and contained 55 photomultipliers. The distance between both heads was 670 mm. In the coincidence mode, lead frames (called scatter frames in the following text) were placed in front of the crystals to suppress the scatter and random background in the field of view from quanta from outside. Both frames reduced the field of view by ~30 mm in the transversal and axial dimensions because of the lead shielding edge. Alternatively, 2 scatter frames configured differently, except for an identical edge thickness, could be chosen. The axial scatter frame used 21 transversally oriented absorbing septa (described by the manufacturer as axial filters), each 5 mm wide and 57 mm deep to divide the axial field of view, thus simulating 2-dimensional PET acquisition with extended septa. The field of view thus consisted of 22 areas, each with a length of 480 mm in transversal and 12 mm in axial dimensions. These transversally oriented septa were missing when the open scatter frame (called open frame by the manufacturer) was used, thus simulating 3-dimensional PET acquisition with retracted septa. While the axial scatter frame was used for acquisition, the entire gantry slowly oscillated in an axial direction to avoid dead zones.

In the coincidence mode, the integration time of the electronic counter was reduced from 850 ns (normal single-photon mode) to 200 ns. The width of the coincidence timing window was 15 ns.

Available acquisition modes are the "list" and the "rebinning-on-the-fly" modes. In the former, the transversal and the axial coordinates and the energies of all coincident quanta pairs are stored sequentially, provided that both quanta energies fall within a predefined interval. In the latter, the coincident pairs are immediately rearranged (rebinned) into virtual parallel projections. In list mode acquisition, this rebinning must be performed subsequently. As with a SPECT camera, the user must choose a sampling angle increment (for a total sampling angle of 180°) and an acquisition time per camera-head rotation angle. A decay correction mode that prolongates the acquisition times for subsequent camera-head rotation angles can be activated to compensate for counting-rate loss resulting from radioactive decay.

The detection probability of a coincident quanta pair depends on the transversal and axial coordinate of origin of the radiation. A geometric correction of pixel counting rates in all virtual parallel projections is therefore performed after the rebinning process.

Before the rebinning is performed, the following parameters must be set to sort out the annihilation events for image reconstruction: amount of geometric acceptance in the transversal and axial orientation, zoom, width of the photopeak energy or Compton energy window, number of virtual parallel projections, and matrix dimension. The number of all coincident pairs rebinned into parallel projections is thus a function of these rebinning parameters and is a subset of the total number of coincident pairs stored during the list mode acquisition.

At the time this article was prepared, no algorithm was available that could perform rapid 3-dimensional rebinning. During rebinning into the virtual parallel projection, the algorithm calculates the transversal coordinate of the coincident pair precisely, whereas the axial coordinate is approximated (single-slice rebinning). The axial approximation process assumes that the 2 annihilation quanta hit the detector perpendicularly within the axial acceptance angle. As a consequence, the axial coordinate is only precise in those few cases in which the 2 annihilation quanta originate on the axis of rotation. The axial coordinate of all other pairs is blurred within the acceptance angle, depending on the distance between their origin and the axis of rotation. Therefore, the axial resolution is influenced by the choice of the axial acceptance angle.

The largest selectable acquisition matrix is 256 × 256. With use of the largest possible zoom (zoom = 2), the minimum pixel size is 1.16 mm.

The choice of rebinning parameters and their influence on image quality were of particular interest in this study. The rebinning parameters chosen as standard were an axial acceptance angle of 16° (the coincidence-detection counting rate almost saturates, because of the geometry of the transversally oriented septa), a transversal dimension of the field of view of 480 mm, a photopeak energy width of 30%, and a Compton energy width of 0%. The studies measuring the spatial resolution (the scatter fraction [SF]) were performed with the largest possible zoom, a matrix dimension of 256 × 256, and 180 (and 120) virtual parallel projections, whereas studies determining sensitivity and counting rate were performed with no zoom, a matrix size of 128 × 128, and 180 virtual parallel projections. All other individual choices of rebinning parameters are stated in this article. The spacing between both camera heads was kept constant.

Available reconstruction algorithms were filtered by backprojection with several filters and an iterative reconstruction maximum-likelihood expectation maximization algorithm developed by the manufacturer. Subsequently, a mathematic attenuation correction based on the determination of the body outline can be applied.

Performance Evaluation

To describe the imaging properties of a PET camera, it was necessary first to determine the spatial resolution, the SF, the sensitivity, and the counting-rate response. All studies were performed with ^{18}F.

In the case of spatially small activity concentrations, knowledge of the spatial resolution makes it possible to ascertain down to what object size the image size is exactly reproduced. Reduction in object size to less than the spatial resolution of a camera is accompanied by only slight reductions in image size, and with further reductions in object size the image size remains almost constant (*3,4*). Provided that the spatial resolution is known, it is

possible to estimate below what object size the recovery (RC) factor (the ratio of the activity concentration in the image of an object to its real activity concentration) is less than 1. This critical object size is generally reported to be 2 to 3 times the spatial resolution (*3,4*).

Another important parameter is the SF of a PET camera. Together with random coincidences, scattered coincidences reduce the image contrast and, in combination with the resolution, sensitivity, and counting-rate response of the camera, determine the detectability of small active lesions.

Therefore, spatial resolution, SF, sensitivity, and counting-rate response of the coincidence scintillation camera had to be determined in this study. The RC factors remain to be determined in a later study.

The sources and phantoms used for the measurements were (a) "hard" line source (an activity-filled needle of 0.8-mm inner diameter) in air, (b) a "soft" line source (activity-filled plastic tube of 1-mm inner diameter) inserted in a water-filled standard cylinder (20-cm diameter, 20-cm height), and (c) a homogeneously filled standard cylinder (20-cm diameter, 20-cm height).

The spatial resolutions in the transversal and axial directions were determined by measuring the line sources in axial and transversal alignment, respectively, and reconstructing them with filtered backprojection (ramp filter). The radial offset (ΔR) from the axis of rotation to the needle in air was varied from 0 to 20 cm when acquiring with the smallest pixel size of 1.16 mm. Two-dimensional gaussian distributions were adapted to the transversally reconstructed tomograms of the line sources, and their radial and tangential full width at half maximum (FWHM) values were defined as the corresponding spatial resolutions.

The SF was defined as the ratio of the number of coincidence pairs resulting from scatter to the total number of coincidence pairs (N_0) within the photopeak energy window. In this study, the SF was determined as follows (*5,6*): a profile was drawn in a sinogram of the "soft" line source in water positioned at a radial offset $\Delta r = 0$ (Fig. 1). The maximum was integrated over a 34-pixel (40-mm)-wide symmetric interval (N_{peak}). From this value the background (N_{back}) was approximated and deducted by a trapezoid with the help of the left and right integration border. The scatter and random fraction was calculated using the formula:

$$SF = (N_0 - N_{peak} + N_{back})/N_0.$$

Initially, the scatter of a line source was determined only at $\Delta r = 0$.

An alternative method to determine the scatter and random fractions was applied: a homogeneously filled standard cylinder in axial orientation was imaged over several half-life periods. The left and right tails of the sinogram profiles, indicating the scatter and random background, were extracted and fitted with 1 gaussian distribution. The ratio of the area under the gaussian distribution to the total profile counting rate represented the sum of the scattered and random coincidences. This method was also used to determine the random fraction. For the homogeneously filled standard cylinder, the sensitivity of the coincidence camera using the 2 scatter frames was determined at a very low activity. For this standard cylinder, a study over several half-life periods was performed to document the counting rate of the camera as a function of the activities (with use of the axial scatter frame). All studies were acquired in an energy interval between 250 and 770 keV (100%).

RESULTS

Axial Resolution

The axial resolution, which depends on the chosen axial acceptance angle and on the distance between the activity source and the axis of rotation, was found to be roughly 6 mm for an axial acceptance angle of 2°, and 10 mm for an axial acceptance angle of 16°.

Transversal Resolution

The relationship between selected rebinning parameters and the transversal resolution for both scatter frames is

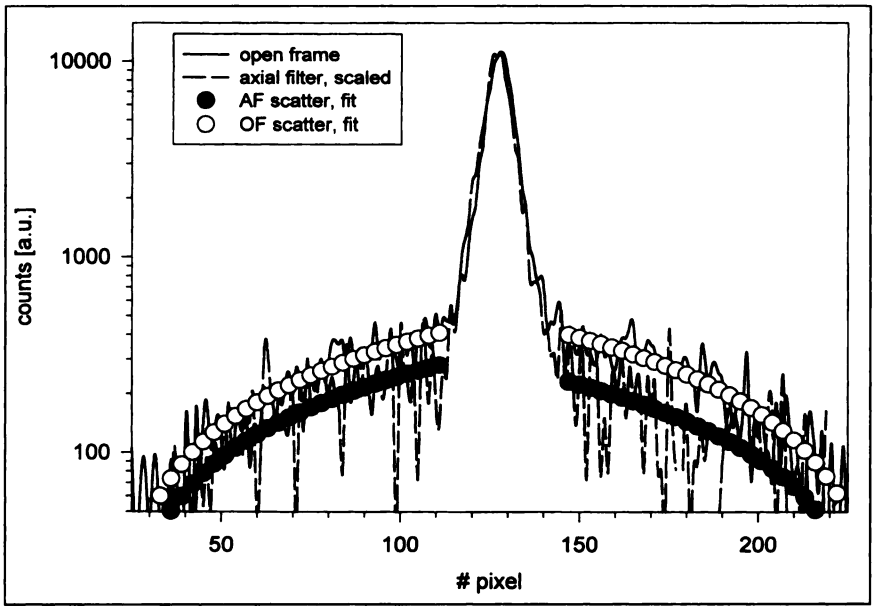

FIGURE 1. Horizontal profiles in sinograms of line source b in water at radial offset $\Delta r = 0$ from axis of rotation. Open (OF) and axial (AF) scatter frames are represented by white and gray lines and symbols. Maxima of 2 profiles have been normalized onto each other, and left and right scatter backgrounds have been fitted with linear functions.

shown in Figures 2–4. Figure 2 shows the x- and y-resolution of the "hard" line source in air as a function of the radial offset (ΔR) from the axis of rotation. The FWHM values rise from 6–7 mm at Δr = 0 cm to approximately 8 mm at Δr = 20 cm. Figure 3 displays both components of the transversal resolution of the "soft" line source in water for both scatter frames as a function of the transversal acceptance of the camera. The y-resolution is generally somewhat worse than the x-resolution. Whereas the transversal resolution is almost independent of the axial acceptance angle, significantly smaller transversal FWHM values were measured when the transversal acceptance was reduced. The loss of transversal resolution with increasing transversal acceptance was probably the result of the reduced detection sensitivity at the ends of the crystal and the geometric correction.

Varying the rebinning parameters not only influenced the spatial resolution of the camera but also the number of coincidence pairs used for image reconstruction (Figs. 4A and B). The number of rebinned coincidence quanta (N_{rebin}) is a subset of all detected coincidence events (N_{tot}); the amount per time and activity concentration is called sensitivity. Therefore, the correlation between spatial resolution and sensitivity was analyzed when only 1 rebinning parameter was varied and all others were kept constant.

Figures 4A and B show the x-component of the transversal spatial resolution as a function of the system sensitivity resulting from differently adjusted rebinning parameters. In Figure 4A only the transversal acceptance was varied. Figure 4B shows the dependence of sensitivity and transversal resolution from the following parameters: axial acceptance, photopeak energy width without Compton energy window, and photopeak energy width of 30% with additional differently adjusted Compton energy widths. The figures show again that a significant improvement in transversal resolution can be achieved only by reduction of transversal acceptance. For example, resolutions of 4–5 mm can be achieved using only the central 100 mm of the transversal field of view during rebinning of coincidence events. However, a reduction in acceptance results in a marked reduction in the sensitivity of the camera with both scatter frames. A considerable increase of system sensitivity was observed not only as the transversal and axial acceptances were raised but also as the selected energy windows were widened.

The relation between the y-component of the transversal resolution and the sensitivity was found to be very similar to that shown in Figure 4.

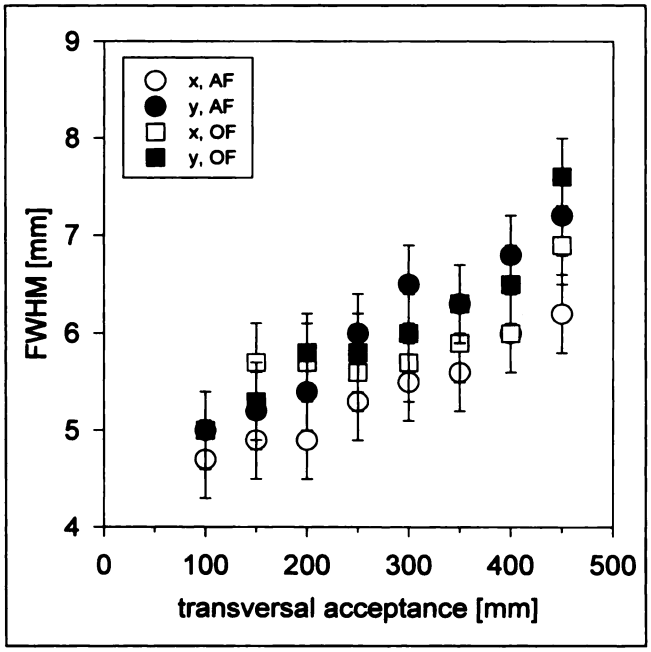

FIGURE 3. Components (x and y) of transversal spatial resolution as function of transversal acceptance of coincidence camera. Line source b in water was measured with axial (AF) and open (OF) scatter frames. Standard rebinning parameters were used, and only transversal acceptance was varied.

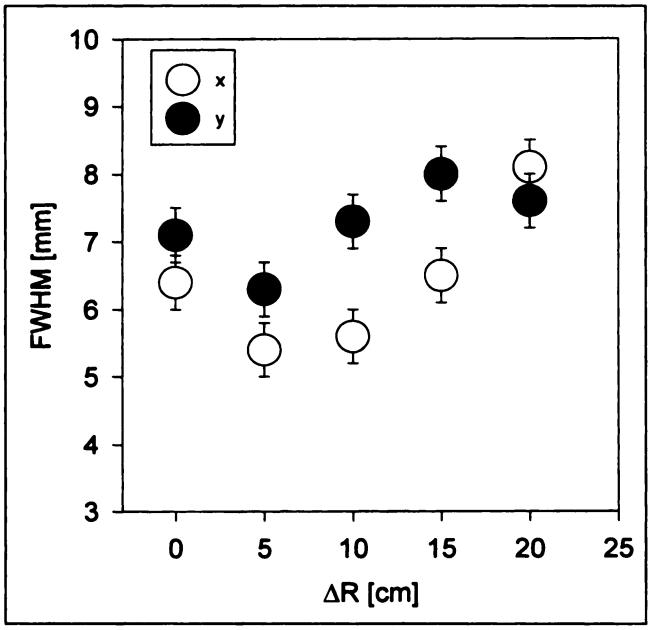

FIGURE 2. Components (x and y) of transversal spatial resolution as function of radial offset ΔR from center of rotation. Line source a in air was measured, and standard rebinning parameters were used. Error bars represent SD of mean after averaging over all transversal slices.

SF

The relationship between the SF in the images and the choice of rebinning parameters was determined for studies with both scatter frames using the line source (b) inserted in a water-filled standard cylinder. In all studies, standardized parameters were chosen during rebinning.

No definite dependence of the SF from the transversal and the axial acceptance could be observed. In studies acquired with the open scatter frame, the SF was about 38%, and it decreased significantly to 25% when the axial scatter frame was used. This is also apparent in Figure 1, which represents

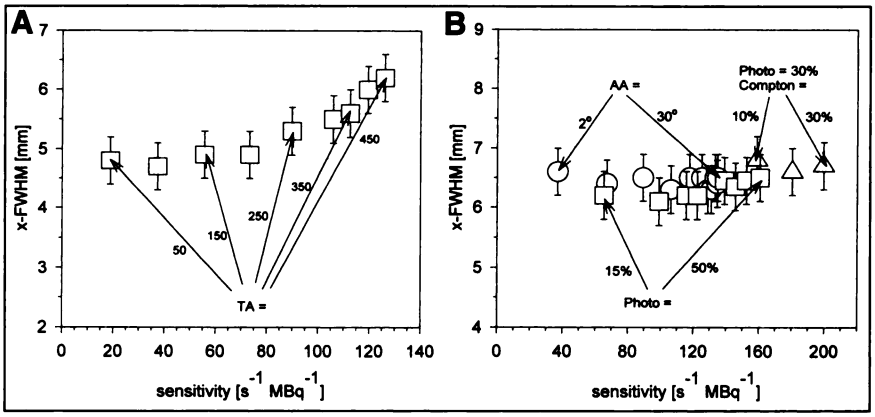

FIGURE 4. (A) Transversal spatial resolution x component correlated with sensitivity of coincidence camera. Transversal acceptance (TA) was varied between 50 and 450 mm; all other rebinning parameters were kept constant. Studies were acquired using axial scatter frame. Identical analysis performed for y component appeared qualitatively similar. (B) Transversal spatial resolution in x direction correlated with sensitivity of coincidence camera. As indicated, axial acceptance (AA), photopeak energy (Photo), and Compton energy (Compton) width were varied individually, whereas other rebinning parameters were kept constant. Studies were acquired using axial scatter frame. Identical analysis performed for y component appeared qualitatively similar.

semilogarithmic profiles in sinograms of the line source (b) in water.

The dependence of SF on the photopeak and Compton energy width used to define coincidence during rebinning is shown in Figures 5 and 6. The use of a Compton energy window in the selection of coincidence events is optional. The objective of its use for image reconstruction is to collect those quanta that are scattered in the crystal but not in the patient. From the larger graph in Figure 5 it can be seen that SF is significantly dependent on the photopeak energy window and can be considerably reduced by decreasing the width. The smaller graph in Figure 5 shows the influence of an optional Compton energy window on SF at a constant photopeak energy width of 30%. Variation of the Compton energy width between 10% and 30% increases the SF from about 28% to 33%.

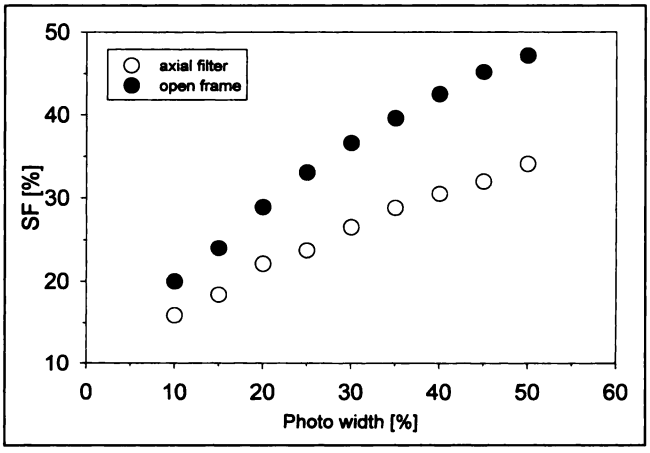

FIGURE 5. Scatter fraction (SF) as function of photopeak energy width (Compton energy width = 0%); other rebinning parameters were kept constant. Smaller inserted graph shows scatter fraction as function of width of Compton energy window, which can be optionally chosen (for photopeak energy width of 30%). Studies were acquired with axial and open scatter frames.

The dependence of the SF in the images on the sensitivity of the coincidence camera with a given choice of rebinning parameters is shown for the axial scatter frame in Figure 6A and for the open scatter frame in Figure 6B. It is clear that SF is influenced only by a variation of the photopeak and/or Compton energy width. Narrowing the photopeak energy width reduces the SF but considerably reduces the sensitivity of the camera, too. The addition of a Compton energy window increases the sensitivity of the camera but also seriously increases SF.

Sensitivity and Counting-Rate Response

The number of all coincidence quanta detected in a 100% (250- to 770-keV) photopeak energy width during list mode acquisition is referred to here as N_{tot}. The number of all coincidence quanta rebinned in a 30% (430- to 590-keV) photopeak energy width is referred to as N_{rebin}.

The sensitivity of the coincidence camera (measured for a standard cylinder homogeneously filled with low activity) is shown in Table 1. Use of the open scatter frame increases the sensitivity by a factor of 6–8 as compared with use of the axial scatter frame.

The counting-rate response as a function of activity is shown in Figures 7A and B using the same homogeneously filled standard cylinder. To estimate random coincidences, a quantification of the sum of scattered and random coincidences was performed by fitting the tails of the sinogram profiles with gaussian distribution. At the present time the camera does not permit determination of random coincidences from the single counting rates of each detector, because their display is not available in the coincidence acquisition mode. From Figures 7A and B it can be deduced that each counting rate reconstructed from this study (the rate of coincidence events detected during list-mode acquisition within a 100% energy window, the rate of coincidence events rebinned within a 30% energy window, the rate of true coincidences, and the rate of random and scattered

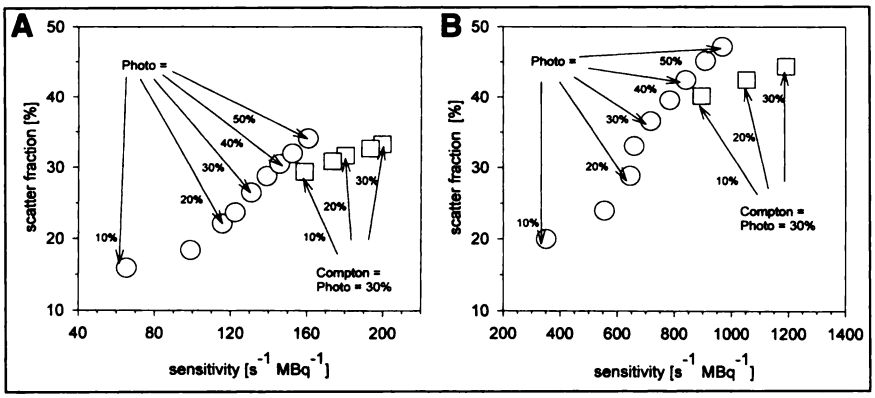

FIGURE 6. (A) SF as function of sensitivity of coincidence camera. Line source b in water was acquired with axial scatter frame. Standardized rebinning parameters were used, and only photopeak energy width (Photo, ○, for Compton energy width of 0%) and Compton energy width, which can be optionally chosen (Compton, □, for photopeak energy width of 30%), were varied. (B) SF as function of sensitivity of coincidence camera. Line source b in water was acquired with open scatter frame. Standardized rebinning parameters were used, and only photopeak energy width (Photo, ○, for Compton energy width of 0%) and optional chosen Compton energy width (Compton, □, for photopeak energy width of 30%) were varied individually.

coincidences) reaches its respective maximum at a different mean activity. The counting rate of true coincidences reaches its maximum at a mean activity that corresponds to roughly 70% of the activity amount at which the counting rate comprised in list-mode acquisition (100% energy width) reaches its maximum. A factory reading in which random coincidences were measured with a delay line showed the real coincidence rate to reach a maximum at approximately 65 MBq for a standard cylinder with use of the axial scatter frame.

DISCUSSION

The spatial resolution of the coincidence camera of 6–8 mm (transversal) and 6–10 mm (axial) for a line source in water is adequate for precise coincidence measurements and is only slightly inferior to high-resolution PET scanners (*7,8*). Given that because of the acquisition programs, the smallest selectable pixel size is only one fifth to one sixth of the spatial resolution of the camera, it can be assumed that spatial resolution determined in this way is somewhat worse than the real spatial resolution. Other reports have recommended that in order to determine the spatial resolution exactly, a pixel size of one tenth of the expected spatial resolution should be selected (*3,4*).

The scatter fractions of approximately 25% in the 2-dimensional mode (axial scatter frame) and approximately 38% in the 3-dimensional mode (open scatter frame) with standard rebinning parameters are relatively high compared with those of conventional 2-dimensional and 3-dimensional PET scanners. A significant reduction in SF can be achieved only by narrowing the width of the coincidence energy window. To date it has not been possible to correct the relatively high SF. At present, random coincidences cannot be measured directly, because in the coincidence mode the single counting rate of the detected 511-keV quanta is not available to the user. Correction for the rate of random coincidences, therefore, is not possible.

TABLE 1
Sensitivity of Dual-Head Coincidence Camera

Frame	Counts per second	N_{rebin} (430–590 keV)	N_{tot} (250–770 keV)
Axial scatter frame	cps/MBq	130	300
	kcps/kBq/mL	30	70
	kcps/MBq/mL	0.8	1.9
Open scatter frame	cps/MBq	750	2460
	kcps/kBq/mL	175	575
	kcps/MBq/mL	4.7	15.5

The sensitivity of the dual-head coincidence camera is distinctly lower than that of PET scanners. When the camera is used with the open scatter frame, its sensitivity is comparable with that of the coincidence camera of another manufacturer (MCD 3D; ADAC Laboratories, Milpitas, CA) (*9*).

The counting-rate response of the camera was determined with the axial scatter frame, only. The maximum counting rate is limited to roughly 2000 true coincidences per second. In this respect the performance of the system is significantly inferior to that of a conventional PET scanner.

In our opinion, it is advantageous that when using the list-mode coincidence acquisition (unlike the rebinning-on-the-fly mode), the rebinning parameters can be optimized after the acquisition. This compensates for the fact that typical list-mode studies are very large (several hundred megabytes).

Variation of the total number of gantry rotations (i.e., variation of the angle increment between 2 gantry angles) showed no consequences in image quality provided that the total acquisition time was kept constant. A sampling with 30 gantry angles and an angle increment of 6° was sufficient for high-resolution images. There were no undersampling effects such as those occurring in conventional PET scanners (*10*).

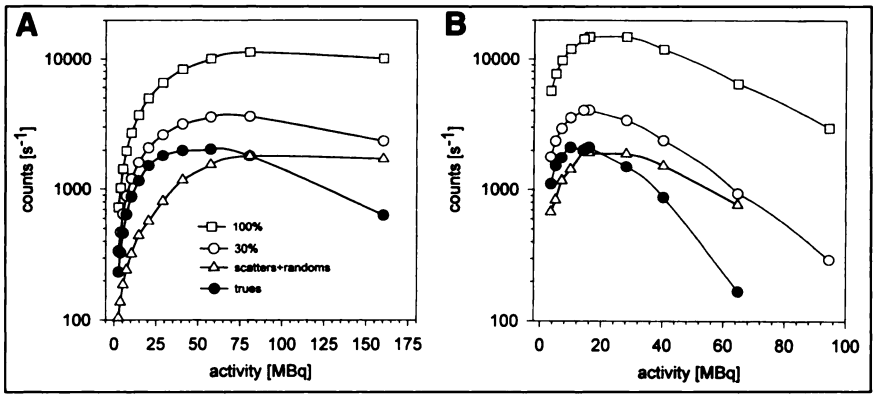

FIGURE 7. (A) Count rates of coincidence camera for hot standard cylinder acquired with axial scatter frame. Count rate of all coincidences detected within 100% photopeak energy window is shown, as is count rate of all rebinned coincidences found within 30% photopeak energy window and count rate of all rebinned coincidences found within 30% photopeak energy window and corrected for scattered and random events (trues). Rate of random and scattered coincidences is also shown. Standardized parameters were chosen for rebinning. (B) Count rates of coincidence camera for hot standard cylinder acquired with open scatter frame. Count rate of all coincidences detected within 100% photopeak energy window is shown, as is count rate of all rebinned coincidences found within 30% photopeak energy window and count rate of all rebinned coincidences found within 30% photopeak energy window and corrected for scattered and random events (trues). Rate of random and scattered coincidences is also shown. Standardized parameters were chosen for rebinning.

Because the attenuation correction is performed only intrinsically and scattered and random coincidences cannot be corrected for, at present there are still some limitations with respect to the quantification of coincidence studies.

Use of the coincidence camera for routine clinical work was found to be satisfactory and stimulating. The camera can be switched very quickly from the single-photon to the coincidence acquisition mode. We have always found this process to be reliable. Because of the 2 acquisition modes, the coincidence camera has become the most frequently used system in our department.

Because inadequate attenuation correction is a major source of errors in quantification, especially in the detection of coincident 511-keV quanta (*11,12*), the effect of attenuation correction by measurement of transmission with an external source must be investigated, because attenuation correction was already implemented by other vendors and is being introduced by Marconi Medical Systems too. Quality control procedures must be defined and standardized. The relatively large active crystal area used in the axial scatter frame and the even larger one used in the open scatter frame demand homogeneity calibration and correction for 511-keV quanta. To achieve quantitatively more precise tomograms, a realistic estimation of random coincidences should be provided. The geometric correction should also be calibrated and could be checked and optimized by regular quality control procedures, ideally in association with homogeneity calibration. The relatively high SF should be reduced with new data acquisition and correction and reconstruction techniques. Newly developed systems will meet at least some of these demands.

CONCLUSION

At present, the coincidence camera is already an appealing device, especially in terms of its usability, both in the single-photon and in the coincidence mode, and its moderate price. A decision on what types of patient examinations the coincidence camera can or should perform on a routine basis therefore must be made soon (*13*). The quanta detection and imaging characteristics of the coincidence camera are inferior to those of conventional PET cameras. Further developments will probably decrease this gap. In view, however, of financial pressure on public health systems even in many developed countries, the potential usefulness of the coincidence camera should not be underestimated. The coincidence camera is a useful complement to, rather than a competitor of, dedicated PET scanners of high resolution and high sensitivity. We expect that the differences that persist between coincidence and PET cameras will become smaller as a result of additional developments in coincidence-detection techniques and, eventually, the use of new scintillation crystals and new detector arrangements (*14*). The development and use of coincidence cameras are undoubtedly interesting variants of PET, stimulating new PET technology.

REFERENCES

1. Budinger TF, Gullberg GT, Huesman RH. Emission computed tomography. In: Herman, GT, ed. *Image Reconstruction from Projection: Implementation and Applications.* Berlin, Germany: Springer-Verlag; 1979:147–246.
2. Picker International, Inc. *Picker Service Manual.* PCD Beta Version. Cleveland, OH: Picker International, Inc., Nuclear Medicine Division; 1997.
3. Spinks T, Guzzardi R, Bellina CR. Measurement of resolution and recovery in recent generation positron tomographs. *Eur J Nucl Med.* 1989;15:750–755.
4. Hoffman EJ, Huang S-C, Phelps ME. Quantitation in positron emission tomography. 1. Effect of object size. *J Comput Assist Tomogr.* 1979;3:299–308.
5. Karp JS, Daube-Witherspoon ME, Hoffman EJ, et al. Performance standards in positron emission tomography. *J Nucl Med.* 1991;12:2342–2350.
6. National Electrical Manufacturers Association. *NEMA Standards: Performance Measurements of Positron Emission Tomographs.* Publication NU 2-1994. Tewksbury, MA: National Electrical Manufacturers Association; 1994.
7. Wienhard K, Dahlbom M, Eriksson L, et al. The ECAT EXACT HR: performance of a new high-resolution positron scanner. *J Nucl Med.* 1994;18:110–118.

8. Bailey DL, Zito F, Gilardi M-C, Savi AR, Fazio F, Jones T. Performance comparison of a state-of-the-art neuro-SPET scanner and a dedicated neuro-PET scanner. *Eur J Nucl Med.* 1994;21:381–387.
9. Schwaiger M, Ziegler S. PET with coincidence camera vs. dedicated ring tomograph: progress or step back? [in German]. *Nuklearmedizin.* 1997;6:3–5.
10. Huang S-C, Hoffman EJ, Phelps ME, Kuhl DE. Quantitation in positron emission tomography. 3. Effect of sampling. *J Comput Assist Tomogr.* 1980;6:819–826.
11. Meikle SR, Dahlblom M, Cherry SR. Attenuation correction using count-limited transmission data in positron emission tomography. *J Nucl Med.* 1993;34:143–150.
12. Huang S-C, Hoffman EJ, Phelps ME, Kuhl DE. Quantitation in positron emission tomography. 2. Effects of inaccurate attenuation correction. *J Comput Assist Tomogr.* 1979;3:804–814.
13. Coleman RE. Camera-based PET: the best is yet to come. *J Nucl Med.* 1997;38:1796–1797.
14. Melcher CL, Schweitzer JS. A promising new scintillator: cerium-doped lutetium oxyorthosilicate. *Nucl Instr Methods Phys Res.* 1992;A314:212–214.